Functional Electrochemistry: On-Nerve Assessment of Electrode Materials for Electrochemistry and Functional Neurostimulation

Jason A. Miranda, Adrien Rapeaux, Isabelle C. Samper, Carolina Silveira, David R. Willé, Gerald E. Hunsberger, Wesley J. Dopson, Huanfen Yao, Annapurna Karicherla, and Daniel J. Chew

***Abstract*—Emerging therapies in bioelectronic medicine highlight the need for deeper understanding of electrode material performance in the context of tissue stimulation. Electrochemical properties are characterized on the benchtop, facilitating standardization across experiments. On-nerve electrochemistry differs from benchtop characterization and the relationship between electrochemical performance and nerve activation thresholds are not commonly established. This relationship is important in understanding differences between electrical stimulation requirements and electrode performance. We report functional electrochemistry as a follow-up to benchtop testing, describing a novel experimental approach for evaluating on-nerve electrochemical performance in the context of nerve activation. An ex-vivo rat sciatic nerve preparation was developed to quantify activation thresholds of fiber subtypes and electrode material charge injection limits for platinum iridium, iridium oxide, titanium nitride and PEDOT. Finally, we address experimental complexities arising in these studies, and demonstrate statistical solutions that support rigorous material performance comparisons for decision making in neural interface development.**

***Index Terms*—Bioelectronics, electrochemistry, electrode materials, nerve stimulation, neural interface.**

***Impact Statement*—This study establishes a repeatable experimental paradigm in which to characterize electrochemical performance of novel electrode materials in the context of nerve activation for bioelectronic medical applications.**

Manuscript received 8 September 2023; revised 26 December 2023 and 15 January 2024; accepted 15 January 2024. Date of publication 22 January 2024; date of current version 23 February 2024. The review of this article was arranged by Editor Paolo Bonato. *(Corresponding author: Jason A. Miranda.)*

Jason A. Miranda is with the Galvani Bioelectonics Ltd., Stevenage, SG1 2NY Hertfordshire, U.K. (e-mail: jason.a.miranda@galvani.bio).

Adrien Rapeaux was with the Galvani Bioelectonics Ltd., Stevenage, SG1 2NY Hertfordshire, U.K. He is now with the Imperial College London, SW7 2BX London, U.K. (e-mail: adrien.rapeaux13@imperial.ac.uk).

Isabelle C. Samper was with the Galvani Bioelectonics Ltd., Stevenage, SG1 2NY Hertfordshire, U.K. She is now with the Global Health Labs, Bellevue, WA 98007 USA (e-mail: isabelle@samper.fr).

Carolina Silveira was with the Galvani Bioelectonics Ltd., Stevenage, SG1 2NY Hertfordshire, U.K. She is now with the Medicines and Healthcare Products Regulatory Agency, E14 4PU London, U.K. (e-mail: carolina.pinto.silveira@gmail.com).

David R. Willé is with GSK PLC, SG1 2NY Stevenage, U.K. (e-mail: david.r.wille@gsk.com).

Gerald E. Hunsberger is with the Galvani Bioelectonics Ltd., Stevenage, SG1 2NY Hertfordshire, U.K. (e-mail: gerald.e.hunsberger@galvani.bio).

Wesley J. Dopson and Daniel J. Chew are with the Galvani Bioelectonics Ltd., Stevenage, SG1 2NY Hertfordshire, U.K. (e-mail: wesley.j.dopson@galvani.bio; daniel.j.chew@galvani.bio).

Huanfen Yao was with the Verily Life Sciences LLC, San Francisco, CA 94080-4804 USA. She is now with the Google LLC, Mountain View, CA 94043 USA (e-mail: claireyao@google.com).

Annapurna Karicherla was with the Verily Life Sciences LLC, San Francisco, CA 94080-4804 USA. She is now with Microsoft Corp., Mountain View, CA 94043 USA (e-mail: anna.karicherla@gmail.com).

This article has supplementary downloadable material available at https://doi.org/10.1109/OJEMB.2024.3356818, provided by the authors.

Digital Object Identifier 10.1109/OJEMB.2024.3356818

I. Introduction

THE expansion of neural interface development for prosthetic limb technologies and bioelectronic therapies highlights the challenges ahead for effective, efficient and durable devices [1], [2]. One of the biggest challenges is activating nerve fibers within heterogenous tissue complexes that may include a mixture of myelinated and unmyelinated fibers, muscle, fat, lymphatic, and vascular tissue [3], [4]. High threshold unmyelinated fibers are of particular interest for developing therapies targeting the autonomic nervous system [5], [6], [7], [8]. These complex targets may require greater levels of charge delivery often surpassing electrochemical limits of commonly used electrode materials. These emerging requirements have stimulated the development and application of novel electrode materials, and the need for a deeper understanding of the functional impact of electrode materials on neural stimulation.

The benchtop electrochemical performance of materials such as smooth platinum iridium (sPtIr), sputtered iridium oxide film (SIROF), titanium nitride (TiN) and poly(34-ethylene dioxythiophene) (PEDOT) have been well characterized [9], [10], [11], [12], [13], [14]. Efforts to standardize characterization methods across research labs have begun, with the aim of accurately supporting the selection of novel materials for novel medical device applications [15]. Electrodes are commonly characterized

for impedance using electrochemical impedance spectroscopy (EIS) and charge injection limits (Q_{inj}) using voltage transients. These tests are usually done in phosphate buffered saline or a model of interstitial fluid as an electrolyte.

On-tissue electrochemistry can differ dramatically from benchtop characterization [10], [16], [17], [18], [19], [20], with impedance increasing and Q_{inj} decreasing in the case of on tissue. Design features also impact the ability of a device to effectively induce action potential generation in nerve fibers including electrode geometry which in turn impacts charge density requirements. Understanding electrochemical performance and charge delivery requirements for nerve activation is important to achieving suitable electrode performance in medical devices. This relationship is currently lacking an agreed understanding, and the development of an experimental platform to compare materials on these metrics, following benchtop characterization, could further strengthen the accurate development of novel electrode materials.

Here we describe a novel experimental approach to evaluate on-nerve electrochemical performance in the context of nerve activation. The electrically-evoked compound action potential (eCAP) provides a broad view of nerve activation thresholds and is used in clinical diagnosis and medical device applications [21]. By directly comparing on-nerve electrochemical performance with eCAP thresholds on an electrode-by-electrode basis, we quantify the therapeutic window and compare well known electrode materials on this metric, revealing clear differences among materials.

Rigorous experimental design is useful for informed decision making in medical device development with regulatory assessment and commercial development reliant on scientifically sound data. Here we demonstrate the use of several statistical approaches and the impact they have on this functional electrochemistry assay and the interpretation of results. For example, quantifying risk can be difficult and subjective, therefore research tools that quantify data in terms of statistical probabilities can be very useful. Such risk-based questions in this context can be:

1) What is the probability that a given electrode material will surpass its charge injection limit before it activates myelinated or unmyelinated nerve fibers?
2) Does this probability depend on charge density factors related to pulse width or amplitude?

A Bayesian framework [22] provides one possible framework to directly answer these questions using data collected from the functional electrochemistry assay. In addition, statistical methods for handling censored data points and sample size estimations are also reported to support future experimental design and aid confident decision making.

II. Methods

A. Electrode Materials

Table I shows electrode materials tested, manufacturers and sample sizes. Up to six electrodes were tested on a single nerve but not all materials were tested on the same nerves. Instead, a smooth platinum iridium electrode was tested on every nerve as a control alongside the test electrode and alternating as the first or last electrode tested. This helped control for variation in nerve size, eCAP amplitude and time since tissue harvest. CorTec cuff electrodes were either used off the shelf or coated with PEDOT (Amplicoat) by Heraeus Medical Components, Germany. Qualia Labs electrodes were placed inside a custom silicon cuff to provide equivalent cuff fit to the CorTec electrodes.

TABLE I
ELECTRODE MATERIALS TESTED ON EX VIVO NERVE

Electrode Material	Source	Electrode surface area (cm^2)	Cuff inner diameter (μm)	Sample size
Smooth PtIr (sPtIr)	CorTec GmbH (Freiburg, Germany)	1.56	800-900	12
Amplicoat™ (PEDOT)	CorTec cuffs PEDOT by Heraeus (Hanau,Germany)	1.56	1000	4
Sputtered IrO_2 Film (SIROF)	Qualia Labs, Inc. (TX, USA)	0.39	750-900	4
Tiatnium Nitride (TiN)	Qualia Labs, Inc. (TX, USA)	0.39	750-900	3

B. Ex Vivo Tissue Preparation

This work was conducted in accordance with Animals (Scientific Procedures) Act 1986, Galvani Policy on the Care, Welfare and Treatment of Animals Policy 040 and approved by the Galvani Bioelectronics Animal Scientific Review Committee and the GSK Policy on the Care, Welfare and Treatment of Animals.

A detailed protocol for the physiological measures has been published elsewhere [23] and described in Supplementary Materials for this manuscript. Sciatic nerves were harvested from 12 adult rats and the mesoneurium was removed at the site of electrode placement. The nerve was transferred to a bath partitioned into two chambers and maintained at 37 °C. In the nerve stimulation chamber, the proximal end of the nerve was submerged in refreshed (5 mL/min) 37 °C modified Krebs-Henseleit buffer (Table S1.) and oxygenated with carbogen. Split-cylinder cuff electrodes were implanted on the thickest part of the nerve in this compartment. The eCAP recording compartment was separated from the buffered Krebs compartment by a silicone grease gap and filled with mineral oil and Ag/AgCl hook electrodes were used to record the eCAP.

C. On-Nerve Electrochemistry and Physiology

Each electrode was evaluated on-nerve for both electrochemical performance and nerve fiber activation thresholds. This allows for a direct comparison of functional electrochemistry across electrode materials. All electrochemical measurements were carried out using a monopolar three-electrode setup with one contact of the implanted cuff as the active electrode, a 2.5 cm × 2.5 cm platinum return electrode (PT000170, Goodfellow Cambridge Ltd., U.K.) and a 2 × 4 mm EP2 Ag/AgCl reference electrode (WPI, USA). Stimulations were delivered using a DS3 Isolated Current Stimulator (Digitimer, U.K.). This

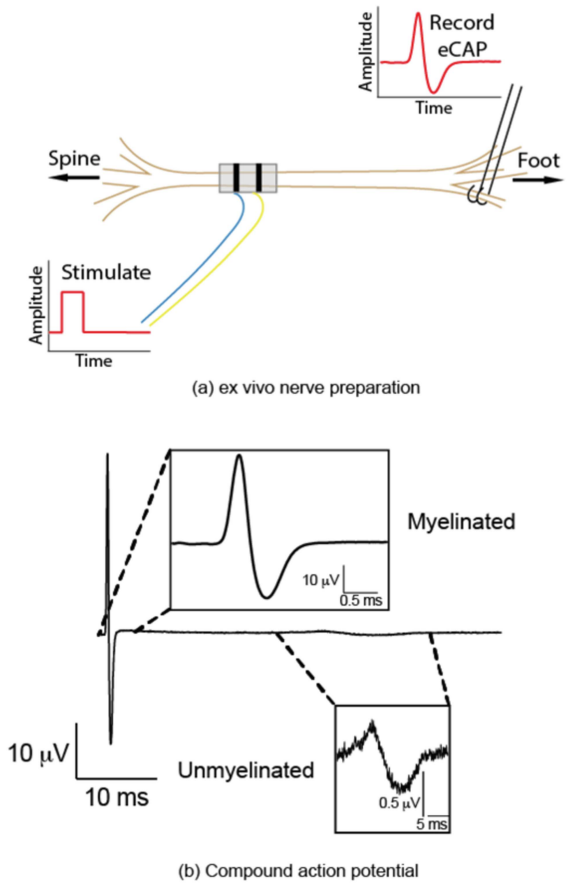

Fig. 1. (a) Ex vivo electrophysiology setup. (b) An example trace of an electrically evoked compound action potential highlighting both fast myelinated and slow unmyelinated responses.

commercially available stimulator was chosen for its fast component rise time during the open circuit potential, experimentally determined to be <10 μs across a 4.8 kOhm resistor at 32 mA (amplitude resulting in the longest component rise time), and wide operational range of current delivery of 2 μA–32 mA. This allows for the same equipment to be used across both low and high threshold nerve fibers and a wide range of electrode sizes and materials, to standardize comparisons over time.

D. Compound Action Potential (eCAP) Threshold

For eCAP stimulation (Fig. 1(a)), monophasic pulses were delivered at pulse widths between 30–3000 μs and between 0.002-32 mA. Stimulation thresholds for myelinated and unmyelinated fibers were determined in response to monophasic pulses for direct comparison with charge injection limits. Details of this procedure are included in Supplementary Materials.

E. Charge Injection Limit

Charge injection limits were determined using negative monophasic voltage transients resulting from rectangular current pulse stimulation delivered between the working electrode and the large platinum counter electrode using the same DS3 stimulator as above. Baseline polarization was determined prior to stimulation, referenced to an Ag/AgCl electrode. The maximum polarization potential, within the water electrolysis window, was measured at 12 μs after the offset of the pulse for the active electrode against the Ag/AgCl reference. A 12 μs timepoint was chosen to ensure the result was not contaminated by the performance of the stimulator as described in Supplementary Materials. Given the use of monophasic stimulation, electrode polarization was allowed to return to the previously determined baseline prior to subsequent stimulations. Electrode voltage transients were recorded using a DC coupled RS PRO RSHS 800 Series isolated oscilloscope (RS, U.K.) or a PicoScope 5444D (Pico Technology, U.K.), connected to a battery powered laptop, for maximum temporal resolution, averaged 4 times to reduce noise. Electrode impedance spectroscopy was also characterized with electrodes on the nerve (Supplementary Materials).

F. Statistical Analysis

Fold change ratios of activation threshold/Q_{inj} were used to quantify the magnitude and direction of the difference between these two measures. Where censored data were present, here values known only to be above a certain value, results were reported using a tobit truncated maximum likelihood method and confirmed by a separate imputation approach using estimates obtained from quadratic regression.

All analyses were performed on a log scale in R [24] using the packages AER [25] for the tobit regression and MCMCpack [26] for Bayesian inference with a normal model and flat priors.

III. Results

A. On Nerve Electrode Performance

Impedance spectroscopy was conducted between 0.3–10 kHz with the electrodes on the nerve to correspond with on-nerve Q_{inj} measures. Impedance profiles were consistent with expectations for the shape of the curves, with sPtIr showing a steep increase at lower frequencies and TiN, SIROF and PEDOT with a more flat, lower impedance profile consistent with increased capacitance of an equivalent Randles circuit (Fig. 2). TiN and SIROF electrodes had higher impedances as expected with lower geometric surface area electrodes (Table I). Electrode materials also differed in surface area-corrected Q_{inj} with PEDOT showing the highest limit (Fig. 2(d)). All materials showed a pulse width dependent Q_{inj} with pulse widths between 0.03–3 ms, as expected [10], with longer pulse widths resulting in higher Q_{inj}.

B. Nerve Fiber Activation

Myelinated and unmyelinated nerve fiber thresholds showed expected response profiles. For rat sciatic nerve, myelinated fibers were activated at lower thresholds with mean charge densities between 1.5 and 44.8 μC/phase/cm^2 (Fig. 2(e)). Unmyelinated fibers showed higher thresholds at mean charge densities between 22.0 and 698.1 μC/phase/cm^2 (Fig. 2(f)). Thresholds also showed a pulse width dependent effect with longer pulse widths resulting in higher activation thresholds for both fiber type. Unmyelinated fiber thresholds showed a surprising difference depending on electrode material with TiN- and SIROF-activated nerves showing lower thresholds at all

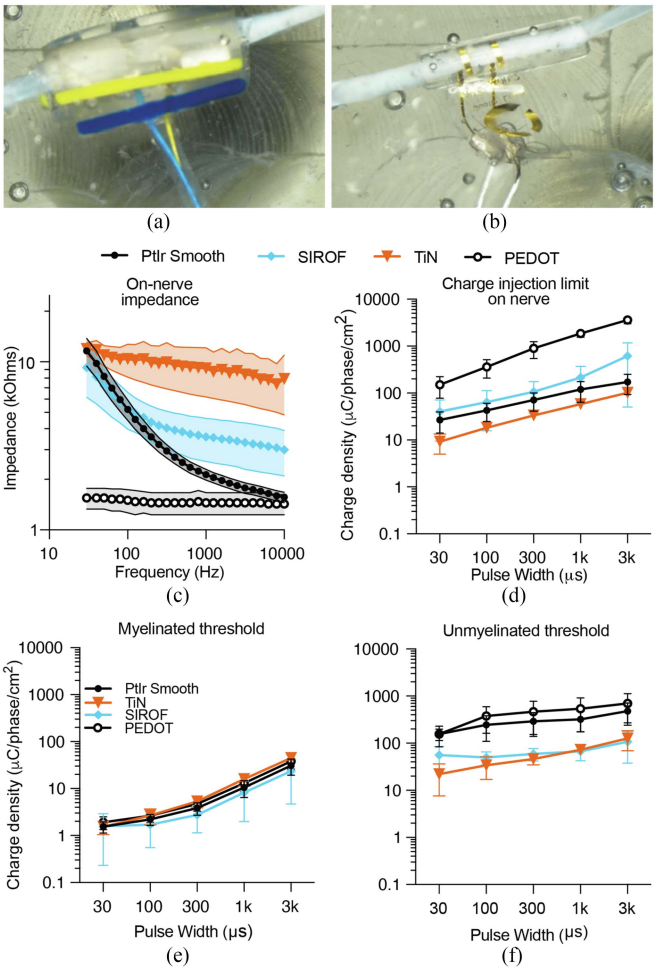

Fig. 2. Electrode characterization profiles for the four materials tested. (a) cuff electrode on ex vivo sciatic nerve representing the cuff form used for PtIr Smooth (n = 12) and PEDOT (n = 4). (b) Cuff form used for TiN (n = 3) and SIROF (n = 4). (c) Electrode impedance spectroscopy. (d) Charge injection limits for different materials at different pulse widths. (e)–(f) Myelinated and unmyelinated fiber thresholds plotted separately for each material. Data points at 30 μs pulse width for two PEDOT and one PtIr preparations in (f) could not be collected due to stimulator limitations (censored data points). Data plotted as mean ± SD.

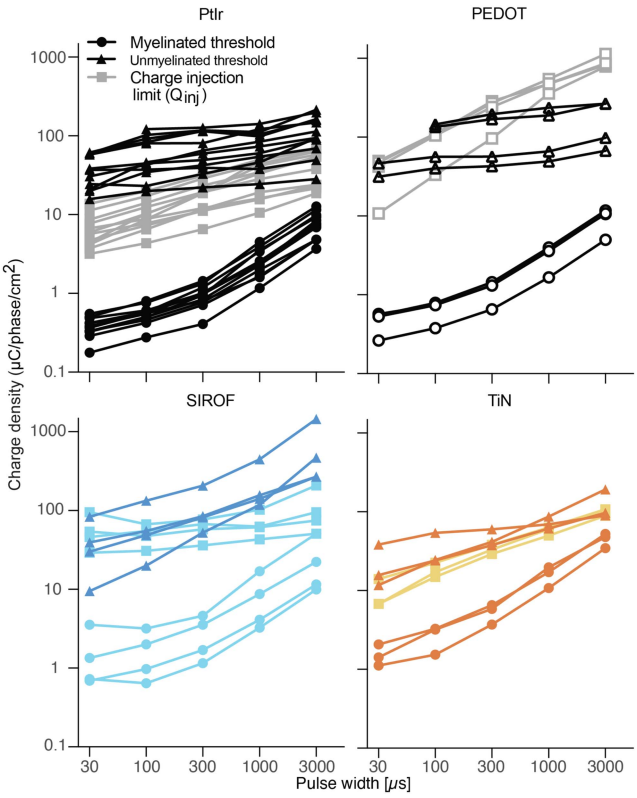

Fig. 3. Individual threshold and charge injection limit curves for all four materials tested. Within a given material graph, three curves are shown for each electrode test (•=myelinated threshold, ▲=unmyelinated threshold, ■=Q_{inj}). Each electrode contained one material type. Some electrodes were tested in multiple ex vivo nerve preparations.

pulse widths. Both of these materials were attached to the nerves using slightly different silicone cuffs (Fig. 2(a), and (b)) and had different electrode geometries, which may have contributed to this effect.

C. Material Charge Injection Limit Relative to Nerve Activation Thresholds

Functional electrochemistry describes the electrochemical performance of an electrode in the context of its ability to activate nerve fiber subtypes. The raw data reveals different functional electrochemistry of materials for activation of high threshold unmyelinated fibers at levels below the Q_{inj} (Fig. 3). Representing these data as a ratio of threshold to Q_{inj} enables quantification of the magnitude of this relationship at each pulse width.

Clear differences in functional electrochemistry ratios were observed, depending on nerve fiber subtype, material and pulse width. All electrode materials achieved myelinated fiber stimulation threshold without exceeding the electrochemical limit at all pulse widths tested (Fig. 4). Q_{inj} ranged between 2.2 and 171.1 times higher than the myelinated fiber threshold, depending on the material and pulse width tested. When a 30 μs pulse width was applied through the material, PEDOT achieved a Q_{inj} 69.5 times higher than activation thresholds and SIROF, sPtIr and TiN between 5.9 and 26.0 times higher. When a 300 μs pulse width was applied, PEDOT achieved a Q_{inj} 171.1 times higher than myelinated fiber activation thresholds. sPtIr and TiN showed reduced separation between Q_{inj} and myelinated fiber activation thresholds at the longest pulse width tested of 3000 μs. Q_{inj} for TiN was 2.2 times and sPtIr 5.4 times higher than activation thresholds.

For the rat sciatic nerve, unmyelinated fibers were activated without exceeding Q_{inj} limit under limited conditions. Q_{inj} ranged between 6.8 times below the fiber activation threshold to 6.3 times higher than threshold, depending on material tested and pulse width (Fig. 4). On average, the sPtIr and TiN tested never achieved statistically significant activation at levels below the Q_{inj}. SIROF and PEDOT did activate unmyelinated fibers at levels below the Q_{inj} for pulse widths of 300–3000 μs. The effect was largest at 3000 μs pulse width, with SIROF activating fibers at 5.0 times and PEDOT at 6.3 times below Q_{inj}.

To directly address the question of how likely a given material is to surpass the Q_{inj} before activating nerve fiber subtypes, a

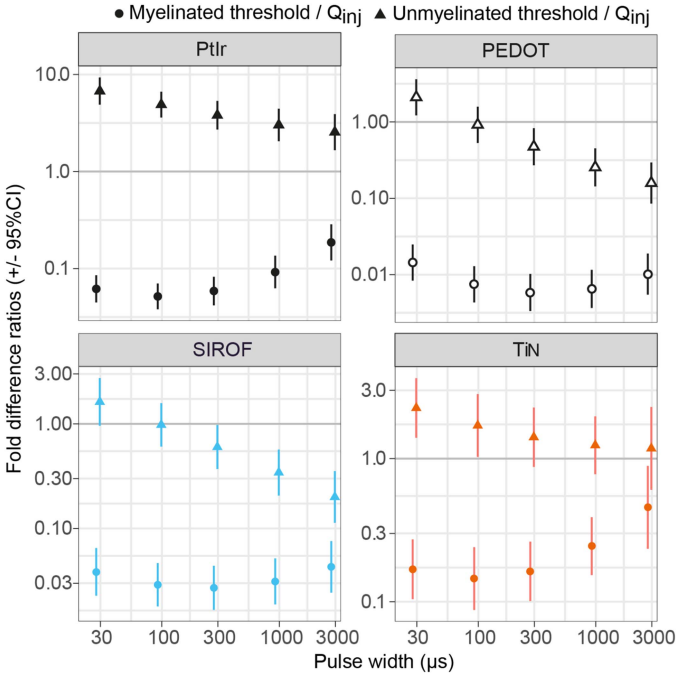

Fig. 4. Functional electrochemistry comparing charge injection limits relative to myelinated (circles) and unmyelinated (triangles) nerve fiber activation thresholds for four electrode materials. Values are represented as ratios of activation threshold/Q_{inj}. Values less than '1' represent conditions where nerve activation occurred within the charge injection limit of a material at a given pulse width. Error bars represent 95% confidence intervals. Analysis was on a log scale. PtIr Smooth n = 12, PEDOT n = 4, SIROF n = 4, TiN n = 3. Censored datapoints from Fig. 3 were imputed using quadratic curve predictions after statistical assumptions were met.

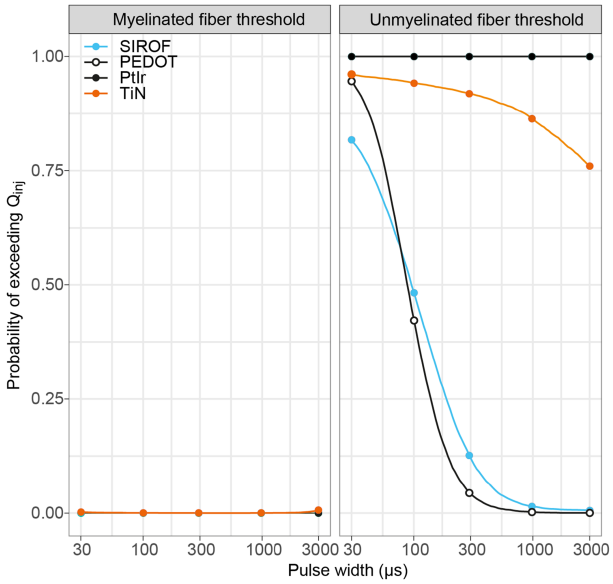

Fig. 5. Chance of exceeding Q_{inj} while activating nerve fiber thresholds. Using a Bayesian model, we estimated the probabilities of exceeding Q_{inj} for the four materials and two nerve fiber types. Probabilities were computed for individual pulse widths and based on values from the quadratic curve fits. Censored datapoints from Fig. 3 were imputed using quadratic curve predictions from adjacent pulse widths.

Bayesian model was used. Using this approach, we see clear differences between materials, placed in a decision-making context. All materials demonstrated a near zero percent chance of reaching Q_{inj} before activating myelinated nerve fibers at all pulse widths, except for TiN that showed a less than1% chance at 3000 μs pulse width (Fig. 5).

For unmyelinated fibers in the rat sciatic nerve, materials differed greatly for this comparison. sPtIr showed a near 100% chance of exceeding Q_{inj} before activating nerve fibers whereas TiN, SIROF and PEDOT all showed a pulse width dependent decrease in probability of exceeding Q_{inj} with longer pulse widths showing lower probabilities. TiN probabilities ranged from 75–95% with 3000 μs demonstrating the lowest. PEDOT and SIROF performed comparably at 30 μs with probabilities of 95% and 80% respectively. Conversely, PEDOT and SIROF demonstrated less than 2% probability of surpassing Q_{inj} before activating unmyelinated nerve fibers at 1000 and 3000 μs pulse widths.

IV. Discussion

Materials used to stimulate neuronal tissue such as peripheral nerves have long been characterized by electrochemical methods with comparisons between materials reported from benchtop characterizations [10] and recent efforts made to standardize biointerface evaluation across research laboratories [15]. Once materials are characterized by these standard methods, additional characterization can deepen the understanding of performance while in contact with the intended target tissue. Several studies have demonstrated that electrochemical properties change when a biointerface is in contact with target tissue [17], [18], [27] with charge injection limit (Q_{inj}) reducing by 17–84%. In our study, Q_{inj} reductions were evident when using cuff electrodes placed around the rat sciatic nerve and stimulation applied. Reductions were of a much smaller magnitude, at around 5% (Fig. S1), when comparing between benchtop electrolyte and on-nerve ex vivo conditions. The high level of variation among studies highlights additional factors that influence performance at the electrode-tissue interface, such as target tissue characteristics. For this reason, it is important to compare material performance in a rigorous and repeatable experimental platform to support the discovery of novel electrode materials. Here, we demonstrate the use of a rat ex vivo sciatic nerve preparation by testing well known electrode materials and setting a foundation on which to compare novel materials.

By comparing electrochemical performance directly with each electrode's ability to stimulate the target nerve fibers, we can evaluate material performance in a controlled context of its intended use and account for some confounding factors. Clear differences emerged among materials when comparing based on functional electrochemistry. sPtIr is expected to perform poorly on Q_{inj} compared to the other three materials and that was demonstrated in this study. On rat sciatic nerves, unmyelinated fibers could not be activated without surpassing the Q_{inj} whereas PEDOT and SIROF could do so for some stimulation parameters. TiN showed an intermediate performance with Q_{inj} and stimulation thresholds statistically indistinguishable

for some parameters. This intermediate performance of TiN is consistent with benchtop characterization [13]. Electrode geometry and geometric surface area also contribute to nerve fiber activation [28] and Q_{inj} [29] which were not ideally controlled for in this study. However, large differences were detected between electrodes of the same geometry (TiN vs. SIROF) demonstrating that these factors were not dominant in determining performance in this study. When using this experimental approach, studies should aim to use the same geometry for all electrodes, where possible, to eliminate this potential source of variation when comparing materials. Alternatively, this approach could be used to determine an optimal geometry in the context of the on-nerve electrochemical performance of a given material by experimentally varying geometry.

All electrode materials showed a pulse width-dependent performance in terms of charge density for both nerve fiber activation thresholds and charge injection limits. This result is consistent with benchtop characterizations of various materials [10], [19]. Shorter pulse widths resulted in lower myelinated and unmyelinated nerve fiber activation thresholds as well as lower Q_{inj}. Regardless of pulse width, all materials activated myelinated fibers below charge injection limits. This is not surprising, as myelinated fibers are low threshold, with stimulation applications targeting neuromuscular and somatosensory needs. The relationship between thresholds and Q_{inj} was non-linear, revealing a pulse width-dependent impact on the ability of materials to activate unmyelinated fibers below the charge injection limit. None of the materials were able to achieve this at pulse widths below 300μs. SIROF and PEDOT activated unmyelinated fibers below their respective Q_{inj} at pulse widths $>= 300$ μs.

The experimental platform reported here can be used in early-stage research to compare novel materials with those more commonly used such as sPtIr. It can also be extended to characterize nerve fiber activation at levels above threshold, up to maximum fiber recruitment. Ultimately, performance in medical devices will depend on the target tissue characteristics and the form factor of the device used to interface with target nerves, resulting in non-linear activation profiles above threshold. For example, the difference in activation profiles can be profound between nerves with mixed fiber diameters, such as the sciatic or vagus nerve [30] and those with homogenous fibers, such as the sympathetic splenic nerve [5]. The same applies for nerve bundles integrated into fatty, musculoskeletal or vascular tissues or organized in a nerve plexus [31], [32]. Furthermore, chronic in vivo implantation impacts electrochemistry depending on fibrotic response and the target tissue [33], [34]. For these reasons, the relationship between activation profiles and Q_{inj} for a given material may be different under different use cases and should be considered separately from this initial rodent nerve screening process.

Together with a rigorous study design and analysis, results from the functional electrochemistry experimental approach can be used to determine quickly, cheaply, and efficiently what electrode materials should be appropriate for specific medical applications. In support of a wider decision-making framework, applying a Bayesian statistical approach to evaluate functional electrochemistry provides a value of the probability for success to be incorporated with other factors such as manufacturability, cost, and durability for the development of medical devices. By establishing similar platforms for a wide range of use cases across labs developing technologies for deep brain, retinal and diffuse nerve plexus stimulation, the field will benefit from a deeper understanding of the factors impacting electrode performance during different types of tissue stimulation.

Supplementary Materials: Supplementary Materials provides details on the experimental setup and electrochemistry methods. Additional results are presented for on benchtop vs. on-nerve Q_{inj}, electrode impedance spectroscopy, and statistical considerations for rigorous experimental design.

Conflict of Interest: The authors declare that the work was conducted in the absence of any commercial or financial conflicts of interest.

Author Contributions: J.A.M., A.R., D.R.W. wrote and D.J.C. edited the manuscript. J.A.M., A.R., D.J.C, A.K., and H.Y. designed the experiments. A.R., I.C.S., C.S. and W.J.D. performed the experiments. D.R.W., A.R., G.E.H and J.A.M. analyzed and interpreted the results. All authors reviewed the manuscript.

ACKNOWLEDGMENT

The authors would like to thank Atefeh Ghazavi and Rylie Green for advice on early stages of this work and George Birkbeck for power calculations.

REFERENCES

[1] M. Cracchiolo et al., "Bioelectronic medicine for the autonomic nervous system: Clinical applications and perspectives," *J. Neural Eng.*, vol. 18, 2021, Art. no. 33592597.

[2] C. Russell, A. D. Roche, and S. Chakrabarty, "Peripheral nerve bionic interface: A review of electrodes," *Int. J. Intell. Robot. Appl.*, vol. 3, no. 1, pp. 11–18, Mar. 2019.

[3] I. Gupta et al., "Quantification of clinically applicable stimulation parameters for precision near-organ neuromodulation of human splenic nerves," *Commun. Biol.*, vol. 3, no. 1, 2020, Art. no. 577.

[4] S. J. Wilks et al., "Non-clinical and pre-clinical testing to demonstrate safety of the barostim neo electrode for activation of carotid baroreceptors in chronic human implants," *Front. Neurosci.*, vol. 11, no. 11, 2017, Art. no. 438, doi: 10.3389/fnins.2017.00438.

[5] M. Donegà et al., "Human-relevant near-organ neuromodulation of the immune system via the splenic nerve," in *Proc. Nat. Acad. Sci.*, vol. 118, no. 20, 2021, Art. no. e2025428118, doi: 10.1073/pnas.2025428118.

[6] D. M. Sokal et al., "Splenic nerve neuromodulation reduces inflammation and promotes resolution in chronically implanted pigs," *Front. Immunol.*, vol. 12, Mar. 2021, Art. no. 649786, doi: 10.3389/fimmu.2021.649786.

[7] C. C. Horn, J. L. Ardell, and L. E. Fisher, "Electroceutical targeting of the autonomic nervous system," *Physiology*, vol. 34, no. 2, pp. 150–162, 2019, doi: 10.1152/physiol.00030.2018.

[8] A. Falvey, C. N. Metz, K. J. Tracey, and V. A. Pavlov, "Peripheral nerve stimulation and immunity: The expanding opportunities for providing mechanistic insight and therapeutic intervention," *Int. Immunol.*, vol. 34, no. 2, pp. 107–118, 2022, doi: 10.1093/intimm/dxab068.

[9] C. Boehler, Z. Aqrawe, and M. Asplund, "Applications of PEDOT in bioelectronic medicine," *Bioelectron. Med.*, vol. 2, no. 2, pp. 89–99, 2019, doi: 10.2217/bem-2019-0014.

[10] S. F. Cogan, "Neural stimulation and recording electrodes," *Annu. Rev. Biomed. Eng.*, vol. 10, no. 1, pp. 275–309, Jul. 2008, doi: 10.1146/annurev.bioeng.10.061807.160518.

[11] S. F. Cogan et al., "Sputtered iridium oxide films for neural stimulation electrodes," *J. Biomed. Mater. Res. Part B: Appl. Biomaterials*, vol. 89, no. 2, pp. 353–361, 2009, doi: 10.1002/jbm.b.31223.

[12] S. Narayan, L. Stoica, A. Liess, and A. Reisinger, "Amplicoat–Conductive polymer coating with enhanced durability and performance for chronic implants," in *Proc. Des. Med. Devices Conf.*, 2021, pp. 1–5, doi: 10.1115/DMD2021-1082.
[13] J. D. Weiland, D. J. Anderson, and M. S. Humayun, "In vitro electrical properties for iridium oxide versus titanium nitride stimulating electrodes," *IEEE Trans. Biomed. Eng.*, vol. 49, no. 12, pp. 1574–1579, Dec. 2002, doi: 10.1109/TBME.2002.805487.
[14] S. J. Wilks, S. M. Richardson-Burns, J. L. Hendricks, D. C. Martin, and K. J. Otto, "Poly(3,4-ethylenedioxythiophene) as a micro-neural interface material for electrostimulation," *Front. Neuroeng.*, vol. 2, 2009, Art. no. 591, doi: 10.3389/neuro.16.007.2009.
[15] A. Weltin and J. Kieninger, "Electrochemical methods for neural interface electrodes," *J. Neural Eng.*, vol. 18, no. 5, 2021, Art. no. 052001, doi: 10.1088/1741-2552/ac28d5.
[16] S. Musa et al., "In vitro and in vivo electrochemical characterization of a microfabricated neural probe," in *Proc. Annu. Int. Conf. IEEE Eng. Med. Biol. Soc., Minneapolis*, 2009, pp. 7143–7146. doi: 10.1109/IEMBS.2009.5335362.
[17] R. T. Leung, M. N. Shivdasani, D. A. X. Nayagam, and R. K. Shepherd, "In vivo and in vitro comparison of the charge injection capacity of platinum macroelectrodes," *IEEE Trans. Biomed. Eng.*, vol. 62, no. 3, pp. 849–857, Mar. 2015, doi: 10.1109/TBME.2014.2366514.
[18] Y. Terasawa, H. Tashiro, Y. Nakano, and J. Ohta, "Safety and efficacy of semichronic suprachoroidal transretinal stimulation with femtosecond laser-induced porosity and smooth-surface electrodes," *Sensors Mater.*, vol. 30, no. 2, pp. 235–249, 2018, doi: 10.18494/SAM.2018.1652.
[19] S. R. Kane, S. F. Cogan, J. Ehrlich, T. D. Plante, D. B. Mccreery, and P. R. Troyk, "Electrical performance of penetrating microelectrodes chronically implanted in cat cortex," *IEEE Trans. Biomed. Eng*, vol. 60, no. 8, pp. 2153–2160, Aug. 2013, doi: 10.1109/TBME.2013.2248152.
[20] S. F. Cogan, "In vivo and in vitro differences in the charge-injection and electrochemical properties of iridium oxide electrodes," in *Proc. Int. Conf. IEEE Eng. Med. Biol. Soc.*, 2006, pp. 882–885, doi: 10.1109/IEMBS.2006.259654.
[21] J. L. Parker, N. H. Shariati, and D. M. Karantonis, "Electrically evoked compound action potential recording in peripheral nerves," *Bioelectron. Med.*, vol. 1, no. 1, pp. 71–83, 2018, doi: 10.2217/bem-2017-0005.
[22] R. Van de Schoot, D. Kaplan, J. Denissen, J. B. Asendorpf, F. J. Neyer, and M. A. G. van Aken, "A gentle introduction to Bayesian analysis: Applications to developmental research," *Child Develop.*, vol. 85, no. 3, pp. 842–860, 2014, doi: 10.1111/cdev.12169.
[23] A. Rapeaux, O. Syed, E. Cuttaz, C. A. R. Chapman, R. A. Green, and T. G. Constandinou, "Preparation of rat sciatic nerve for ex vivo neurophysiology," *JoVE*, no. 185, 2022, Art. no. e63838, doi: 10.3791/63838.
[24] R. Core Team, "*R: A language and environment for statistical computing*," R Foundation for Statistical Computing, Vienna, Austria, 2020.
[25] C. Kleiber and A. Zeileis, *Applied Econometrics with R*. New York, NY, USA: Springer, 2008.
[26] A. D. Martin, K. M. Quinn, and J. H. Park, "MCMCpack : Markov chain Monte Carlo in R," *J. Statist. Softw.*, vol. 42, no. 9, pp. 1–21, 2011, doi: 10.18637/jss.v042.i09.
[27] H. Tashiro et al., "In vitro and in vivo long-term electrochemical properties of electrodes with femtosecond-laser-induced porosity for visual prostheses based on suprachoroidal transretinal stimulation," *Sensors Mater.*, vol. 30, no. 2, pp. 251–268, 2018.
[28] A. Ghazavi, D. Westwick, F. Xu, P. Wijdenes, N. Syed, and C. Dalton, "Effect of planar microelectrode geometry on neuron stimulation: Finite element modeling and experimental validation of the efficient electrode shape," *J. Neurosci. Methods*, vol. 248, pp. 51–58, 2015, doi: 10.1016/j.jneumeth.2015.03.024.
[29] R. A. Green, H. Toor, C. Dodds, and N. H. Lovell, "Variation in performance of platinum electrodes with size and surface roughness," *Sensors Mater.*, vol. 24, no. 4, pp. 165–180, 2012, doi: 10.18494/sam.2012.821.
[30] M. L. Settell et al., "Functional vagotopy in the cervical vagus nerve of the domestic pig: Implications for the study of vagus nerve stimulation," *J. Neural Eng.*, vol. 17, no. 2, Apr. 2020, Art. no. 026022, doi: 10.1088/1741-2552/ab7ad4.
[31] W. M. Grill, "Modeling the effects of electric fields on nerve fibers: Influence of tissue electrical properties," *IEEE Trans. Biomed. Eng.*, vol. 46, no. 8, pp. 918–928, Aug. 1999, doi: 10.1109/10.775401.
[32] H. Ye, M. Cotic, M. G. Fehlings, and P. L. Carlen, "Influence of cellular properties on the electric field distribution around a single cell," *Prog. Electromagn. Res. B*, vol. 39, no. 39, pp. 141–161, 2012.
[33] J. C. Williams, J. A. Hippensteel, J. Dilgen, W. Shain, and D. R. Kipke, "Complex impedance spectroscopy for monitoring tissue responses to inserted neural implants," *J. Neural Eng.*, vol. 4, no. 4, pp. 410–423, 2007.
[34] A. R. Harris, C. Newbold, D. Stathopoulos, P. Carter, R. Cowan, and G. G. Wallace, "Comparison of the in vitro and in vivo electrochemical performance of bionic electrodes," *Micromachines*, vol. 13, no. 1, pp. 1–17, 2022.
[35] K. S. K. Lau, T. Chen, S. N. Iwasa, M. Volpatti, M. R. Popovic, and C. M. Morshead, "A novel ex vivo assay to define charge-balanced electrical stimulation parameters for neural precursor cell activation in vivo," *Brain Res.*, vol. 1804, no. 1, 2023, Art. no. 148263.
[36] J. Li, X. Kong, S. N. Gozani, R. Shi, and R. B. Borgens, "Current-distance relationships for peripheral nerve stimulation localization," *Anesth. Analg.*, vol. 112, no. 1, pp. 236–241, 2011.